International Journal of Environmental Sciences
ISSN: 2229-7359
Vol. 11 No. 2, 2025
https://www.theaspd.com/ijes.php

Controlled Crystallinity of SnO_2 Nanoparticles Through Solvent Engineering and Thermal Treatment

Jitender Josun[a,] *, Praveen Sharma[a], Vinod Kumar Garg[a,b]

[a] Department of Environment Science and Engineering, Guru Jambheshwar University of Science and Technology, Hisar 125001, Haryana, India

[b] Centre for Environmental Sciences and Technology, Central University of Punjab, Bathinda 151001, Punjab,
India

***** Corresponding author
Email addresses: simonejosun21@gmail.com

Abstract

SnO_2 nanocrystals were engineered by sol-gel calcination in mixed solvent systems (methanol: ethylene glycol: water) and fired at 550 °C and 750 °C. Structural analysis by X-ray diffraction revealed phase-pure, tetragonal rutile SnO_2 with a pronounced (110) texture. Crystalline diameters increased from 19.2 → 21.8 nm (550 °C) and 27.4 → 30.1 nm (750 °C) as water content rose. FESEM imaging revealed morphological evolution from smaller, less-agglomerated particles in organic-rich media to larger, aggregated structures in aqueous-rich systems. EDX verified stoichiometric Sn and O, while FTIR displayed strong Sn–O vibrations (622–668 cm^{-1}). DRS-UV-Vi's spectra showed excitonic onsets red-shifted beyond bulk SnO_2 (344 nm), with band-gap energies narrowing modestly as organic content declined—consistent with minimal quantum-confinement effects at the measured sizes. Overall, solvent polarity proved decisive: organic-rich media favoured smaller, less-agglomerated crystals, whereas water promoted growth. Tailoring solvent composition and calcination temperature therefore enables controlled size, morphology, and high-energy-plane exposure, providing a straightforward route to SnO_2 nanomaterials optimized for visible-light photocatalysis.

Keywords: *SnO_2, Organic solvents, Texture coefficient, Sol-gel calcination, Optical bandgap, Crystalline size, Tauc's Plot.*

INTRODUCTION

Exploration of materials and their characteristics down to the nanoscale has been driven by the fascination of scientists worldwide with metal oxide semiconductor nanoparticles, including TiO_2, SnO_2, CuO, and ZnO. From a scientific point of view, these materials are crucial, and they have a wide variety of purposes; for example, in electronics [1], photovoltaic conversion [2], optoelectronics [3], and silicon solar cells [4]. With a vast exciton binding energy of 130 meV and a broadband gap of 3.6 eV at 330 K, tin oxide is among the best and most efficient n-type semiconductor oxides [5]. Lattice parameters of tin oxide are a = b = 4.74, c = 3.19 and highly transparent in the visible region (>80%) [6]. There are several commercial applications for SnO_2 because of its, excellent availability, great sensitivity, non-toxicity, cheap cost and chemical and thermal resilience. Its electrical, catalytic, and optical capabilities are intriguing and might lead to its use in many applications. For example, tin oxide may be used as a gas sensor in ceramics [7-8], a dye-based solar cells [9], a support for catalysts [10], a field effect transistor [11] a transparent conducting oxide [12], and a substance for the anode of lithium-ion batteries [13]. Nanostructured materials' beneficial properties and applications depend highly on their chemical composition, size, shape, and structure. Some researchers have demonstrated that the size and shape of nanoparticles may be affected by factors such as the surrounding temperature, the number of precursors, the capping molecule, the solvents used, and the passage of time [14].

Solvents play a key role in controlling reaction temperature by setting the maximum limit at which the reaction can proceed. Since the solvent's polarity affects the nucleation and growth of SnO_2NP's on their different faces, it was hypothesised that this property primarily determines the

particle size and shape with the aspect ratio. The growth rate of a crystal face is typically influenced by a combination of internal factors, such as dislocations and intermolecular interactions, as well as external variables, including reagent type, temperature, solvents, mineralizers, and impurities [15]. Prior research has revealed that the growth and coarsening of particles are significantly influenced by the versatile properties of the solvent, including its viscosity, bulk solubility, and surface energy [16]. This versatility allows us to use various solvents, thereby regulating the size and distribution of SnO_2 nanoparticles. Controlling these properties is crucial for changing their optical, electrical, chemical, and magnetic characteristics, opening up new scientific research opportunities. Ultimately, the synthesis process determines many technical characteristics that affect the practical performance of SnO_2, including crystallinity, surface morphology, crystal size, lattice parameters, optical band gap and texture coefficient.

Numerous researchers have developed scientific methods for synthesising SnO_2 nanoparticles, including chemical vapour deposition, physical vapour deposition, thermal evaporation, thermal decomposition [17], hydrothermal [18], microwave [19], and sonochemical methods [20]. These methods typically require high operating temperatures, leading to increased energy consumption. Additionally, they tend to be expensive due to the specialized equipment and materials needed, and their processes are often intricate, involving multiple steps and precise control of conditions. Sol-gel calcination is an alternative to traditional methods for synthesising tin oxide nanoparticles. It allows for precise control of particle size, shape, and dispersion. This process offers a few benefits, including low temperature, homogeneity, phase-pure powders, minimal danger, high efficiency, homogeneity, and high purity. It is also environmentally friendly [16].

A multitude of studies have been conducted, each exploring the effects of solvents on growth and material properties, employing a variety of methods. A simple solvothermal synthesis using a mixture of Ethylenediamine (EN) and distilled water resulted in various ZnS morphologies. The impact of the solvent medium on ZnS nanoparticles' structural, morphological, and optical features was examined. Results indicate the effective production of hexagonal ZnS nanorods in a mixed solvent. Mendil et al. [21] discovered that increasing the percentage of Ethylenediamine (EN) in the solvent increased the band gap of ZnS from 3.49 to 3.74 eV. Paloly and Bushiri [22] investigated how solvents affected the tin oxide thin films deposited by chemical spray pyrolysis, their growth, and essential characteristics. The results demonstrated that methanol, followed by ethanol, was used as a solvent precursor to create SnO_2 thin films for use in TCO applications. Researchers Ungula and Dejene [16] used the sol-gel technique to examine how different solvent media, including water and ethanol, affected the optical, morphological, and structural characteristics of ZnO nanoparticles. The findings were that a lower band gap and smaller crystalline size were observed when the volume ratio of ethanol in the solvent increased. The synthesis medium influences the optical characteristics of these materials. The co-precipitated method's impact on tin oxide's structure, morphology, and optical characteristics as a function of solvent media (methanol: water). According to the findings presented by Kumar et al., [23] the optical energy gap of SnO_2 dropped from 3.66 eV to 3.54 eV as the methanol to water solvent ratio declined, and the particle size reduced as the methanol to water ratio increased. Khoza et al. [14] demonstrated how the morphological and photonic characteristics of HDA-capped ZnO nanoparticles produced by microwave irradiation are affected; the researchers investigated the effects of various polarities of solvents, including water, ethanol, and acetone. These studies show that hydroxyl groups in water and ethanol interact with nanoparticles throughout their life cycle, from nucleation to growth and termination, resulting in non-spherical morphologies. Conversely, rods with a high aspect ratio were produced by both acetone and ethanol. These findings, meticulously obtained, contribute significantly to our understanding of the effects of solvents on nanoparticle morphology. Khan et al. [24] examined the influence of polar-aprotic solvents (acetonitrile, DMF, DMSO, and 1,4-dioxane) and polar-protic solvents (methanol, ethanol) on the size distribution and optical absorption spectra of surfactant-stabilized silver nanoparticles. The reducing agent and stabilizing agent, respectively, were CTAB. The data reveal that (i) when the dielectric constant of the medium and surface-adsorbed species increases, the absorbance falls. (ii) Particle size rises when methanol and ethanol molecules are added. (iii) The absorbance is reduced by lowering the growth rate when acetonitrile, dimethylformamide,

dioxane, and dimethylsulfoxide are added. (iv) The absorbance remains relatively unchanged at higher concentrations of solvents.

Most of these studies concentrate on co-precipitation, spray pyrolysis, microwave irradiation methods, and the usage of CTAB-Ag, ZnS, ZnO thin films, and SnO_2 thin films. Only a limited number of solvents and approaches are employed for comparison. There is currently no comprehensive study in the literature that compares the effects of various calcination temperatures with solvent volume ratios (methanol: ethylene glycol: water) on SnO_2 nanocrystalline via the sol-gel-calcination process. The synthesized SnO_2 nanoparticles are compared with other researchers' results in Table 5. This study is not just about creating a nanocrystalline SnO_2 structure but about doing so in an energy-efficient manner. The sol-gel-calcination technique is our tool, and this study investigates the impact of varying precursor volume proportions of solvents with calcination temperatures on the crystallographic structure, morphology, optical, functional groups, and dispersive properties. The synthesized SnO_2 nanoparticles are crucial for future studies because they can serve both as adsorbents in adsorption and as a catalyst to increase photocatalytic activity to remove dyes.

2. MATERIALS AND METHODS

All Analytical grade reagents (AR) were supplied from Sigma Aldrich without additional purification before utilisation. The Tin dichloride dihydrate (98 %, $SnCl_2.2H_2O$) as a Sn-precursor and aqueous ammonium solution (25%, NH_3 (aq.)) were considered. Methanol (CH_3OH), Ethylene glycol ($C_2H_6O_2$) and DDW (Double distilled water) were utilised as solvents in the synthesis process. Ethanol (C_2H_5OH) was used for purification of SnO_2.

2.1 Synthesis of Tin Oxide (SnO_2) nanoparticles

The sol-gel-calcinations process of synthesized SnO_2 nanostructures at different temperatures and volume ratios of solvents is shown in Table 1. The desired concentration of 0.25 M (5.641 g) of tin dichloride dihydrate was dissolved in mixed solutions of different solvent media ratio (methanol: ethylene glycol, methanol: ethylene glycol: water and ethylene glycol: water) in a 250 ml volumetric flask by magnetically stirred for 15 min to make a 100 ml transparent homogeneous precursor mixture. Aqueous ammonia was gradually introduced to the mother solution until the pH reached 10, under magnetic stirring for 30 minutes at 40 °C, leading to precipitate formation. Fig. 2 depictsthe chemical reaction and the solutions appeared pale yellowish color. During the process, products were immersed into an ultrasonic wave cleaner at 80 ºC for 2 hrs and then kept at room temperature for the next 22 hrs to ensure homogeneous mixing. The resulting precipitates were again sonicated for 30 min to minimize particle agglomeration, and then repeatedly washed with double-distilled water and ethanol to eliminate residual ions to reach pH 7. The thoroughly washed precipitates were dried in a hot-air oven at 80 °C for 2 hrs and subsequently calcined at 550 °C and 750 °C for 2 hrs using a muffle furnace. Grinding it to a fine consistency in an agate mortar yielded a greyish powder. The characterization tests were conducted on greyish-colored powdered SnO_2 nanoparticles and designated with markings such as S1-550, S1-750, S2-550, S2-750, and S3-550, S3-750, as shown in Fig. 1.

Table 1. Preparation Conditions of SnO_2 Nanoparticles.

Processing Code	Chemical precursor (100 ml)	Volume Ratios of solvents (Methanol: Ethylene glycol: DDW)	Ammonia solution (25%)	Temperature (^OC)
S1	0.25 M	50:50:0	5 ml	550, 750
S2	0.25 M	25:25:50	5 ml	550, 750
S3	0.25 M	0:0:100	5 ml	550, 750

International Journal of Environmental Sciences
ISSN: 2229-7359
Vol. 11 No. 2, 2025
https://www.theaspd.com/ijes.php

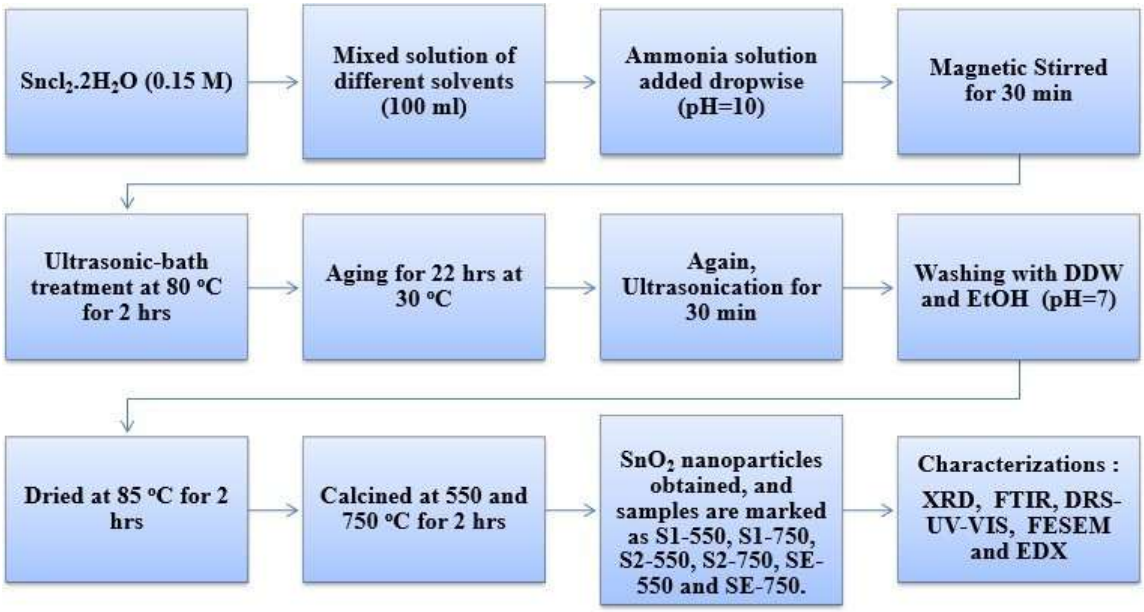

Fig. 1: Flow Chart of Synthesized SnO_2 nanoparticles by sol-gel assisted calcination process.

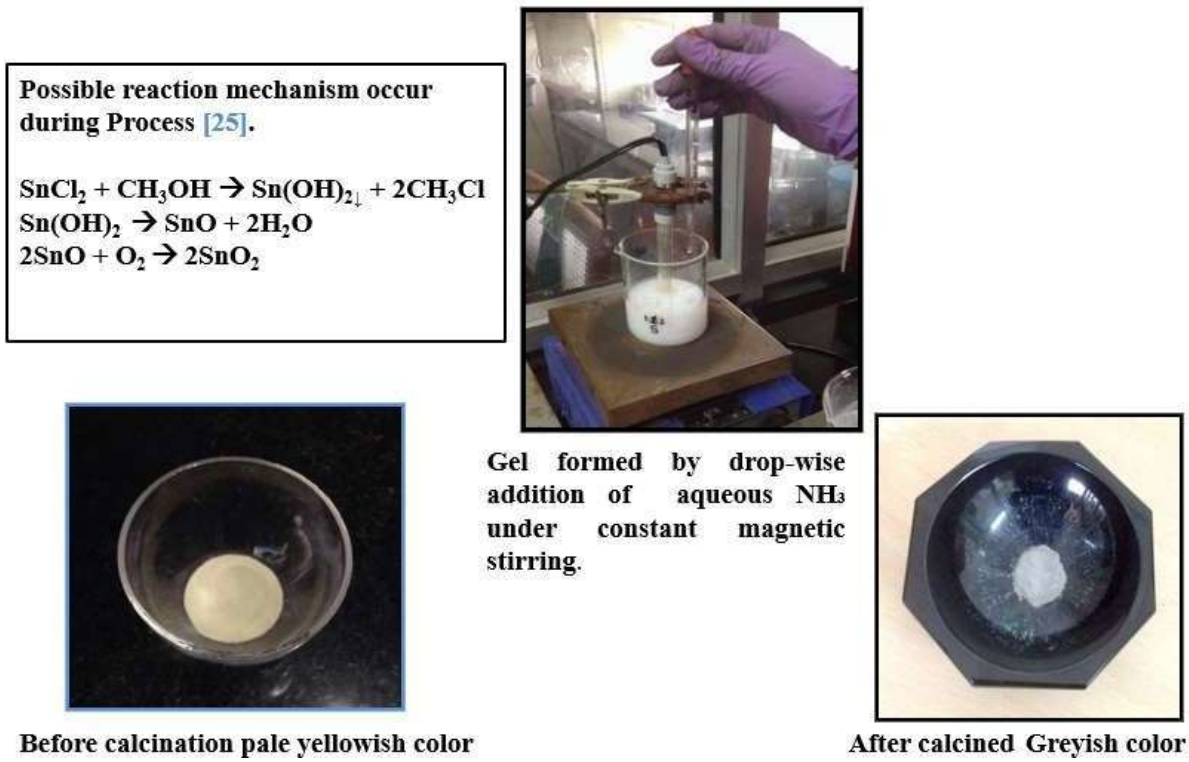

Fig. 2: Photographic illustration of synthesized SnO_2 nanoparticles and reaction process.

2.2 Characterizations for SnO_2 nanoparticles

Various characterization approaches, including XRD, DRS-UV-VIS, FTIR, FESEM, and EDX, were employed to detect and confirm the presence of compounds in the as-synthesized SnO_2 samples at varying calcination temperatures and organic to water solvent media. The crystallographic properties of SnO_2 samples were analyzed using an X-ray diffractometer (XRD, Rigaku Miniflex II) with CuKα radiation (λ = 1.54 Å), operated at 30 kV and 15 mA. The data were collected at a scan speed of 2°/min over a 2θ range from 20° to 80°. The shape and size of SnO_2nanoparticles were analyzed by Field emission scanning electron microscopy (FESEM, QUANTA, and FEG-450) at different magnifications. The elemental composition of the nanoparticles was analyzed through energy-dispersive X-ray spectroscopy (EDX) coupled with field-emission scanning electron microscopy (FESEM) for comprehensive characterization. The Fourier transform infrared spectroscope (FTIR) spectroscopy (Perkin Elmer Spectrum BX-II) was performed using KBr pellets, with spectra recorded in the 4000 cm^{-1} to 400 cm^{-1} range to analyze the functional groups of the nanoparticles. The optical absorbance of SnO_2 nanoparticles was analyzed using UV-Vis diffuse reflectance spectroscopy (DRS, SHIMADZU UV-2600) in the 200 to 800 nm range. Barium sulphate ($BaSO_4$) was used as a reference to account for the reflectance of the samples.

3. RESULTS AND DISCUSSION

3.1. XRD analysis

The crystallographic structures of all tin oxide (SnO_2) nanoparticle samples were examined using XRD patterns. The samples (i.e. S1-550, S1-750, S2-550, S2-750, and S3-550, S3-750) that were sol-gel-calcinated with different solvent volume ratios (methanol: ethylene glycol: water = 50:50:0 (S1), 25:25:50 (S2), and 0:0:100 (S3)) were subjected to heating at temperatures of 550 °C and 750 °C respectively, as illustrated in Fig. 3. The sharp and intense diffraction peaks of all samples of SnO_2 nanoparticles for 2θ values were located at around 26.51°, 33.82°, 37.90°, 51.70°, 54.76°, 57.76°, 61.88°, 64.74°, 65.86°, 71.20°, and 78.64° with miller indices (hkl) assigned to planes (110), (101), (200), (211), (220), (002), (310), (112), (301), (202), (321) respectively. The detected peaks match the tetragonal rutile structure of SnO_2 nanoparticles, closely aligning with the standard values for bulk SnO_2 (JCPDS card no. 00-021-1250), where a = 0.4738 nm, c = 0.3188 nm, and c/a = 0.672. The experimentally determined d-spacing values match those reported in JCPDS card no. 00-021-1250, confirming the accuracy of the crystal structure. The XRD pattern did not show any additional impurity peaks, suggesting that all SnO_2 nanoparticle samples were synthesised with a high level of purity. As illustrated in Fig. 3, the (110) peak was the most prominent at 2θ for all SnO_2 samples. This peak showed much greater intensity than the (101) and (211) peaks, suggesting a preferential crystallographic orientation along the (110) plane. This alignment is further validated by the texture coefficient (Table 2). The XRD results showed that the intensity of the diffraction peaks increased with an increase in the water content of the solvent medium and with an increase in the calcination temperature of SnO_2 nanoparticle samples. Table 3 summarises the summed data for all parameters of all SnO_2 nanoparticle samples. To calculate lattice parameters (a) and (c) and the unit cell volume on crystal planes in the tetragonal rutile structure of SnO_2 by using the following equations (Eq.1,2) [3,6].

$$\frac{l}{d_{hkl}^2} = \frac{h^2+k^2}{a^2} + \frac{l^2}{c^2} \quad (1)$$

$$V = a2c \quad (2)$$

Here, (hkl) represents the lattice plane of Miller indices; the 'a' and 'c' are crystal lattice constants (nm); d_{hkl} is the inter-planar distance (nm), and V is the unit cell volume ($Å^3$) on crystal planes. Bragg's law (nλ = 2dsinθ, n = 1) relates the X-ray wavelength (λ = 0.154 nm), diffraction angle (θ), and interplanar spacing (d). Using this equation (Eq. 3), the interplanar spacing (d, in nm) can be determined from the diffraction data [26].

$$d = \frac{\lambda}{2 \sin \theta} \quad (3)$$

Table 3 shows that the values of lattice parameters (a) and (c) of all samples of SnO_2 nanoparticles were closer to the reference file data values of bulk SnO_2 with an interplanar d-spacing value of~ 0.3357 nm at the plane (110). The c/a ratio of 0.672 aligns with the expected value for an ideally close-packed tetragonal structure, indicating a well-ordered crystal arrangement. The values of the lattice parameters exhibited minor variations among the samples fabricated at 550 °C and 750 °C using distinct solvent volume ratios. A proportional reduction in the volume of the unit cells was also observed as the water content ratios and calcination temperatures were elevated. However, the obtained values of unit cell volume on crystal planes for all the samples of SnO_2 were nearer to the reported data of bulk SnO_2 (i.e. 71.57 $Å^3$). It could result from a multitude of defects, including local lattice disorder, Sn interstitials, vacant lattice sites and surface defects [23]. Consistent results have been observed in the literature, as reported by Ungula and Dejene [16] and Chand [27], supporting these findings. Furthermore, microstructural characteristics, including dislocation density and number of unit cells, have been estimated in the following relations for enhanced XRD analysis (Eq. 4, 5) [6, 28].

$$\delta = \frac{1}{D^2} \quad (4)$$

$$n = \frac{\pi D^3}{6V} \quad (5)$$

Where, δ stand for dislocation density (lines/m^2) (x 10^{15}); D symbolize for crystalline size (Å); n is number of unit cell (x 10^3); Pie is constant value (π =3.14).

Dislocation density is also an essential factor in investigating the growth mechanisms. Dislocation density (δ) is inversely related to particle size and the number of unit cells. It reflects the length of dislocation lines per unit volume (lines/m2) within the crystal structure, providing valuable insights into crystal imperfections [29]. Table 3 displays the data for all SnO_2 nanoparticle samples. As the water content in the solvent medium and the calcination temperatures increased, the dislocation density decreased, and the number of unit cells increased. Consequently, this led to enhanced crystal growth and a reduction in defects within crystallites, and the crystalline size became larger [28]. The mean crystalline size (D in nm) of SnO_2 nanoparticles was calculated from the broadening of diffraction peak (110) by using Debye Scherrer's equation (Eq.6) as follows [6].

$$D = \frac{k\lambda}{\beta \cos \theta} \quad (6)$$

Where λ is the CuKα wavelength (0.15406 nm), k is Scherrer's constant (0.9), β is the FWHM at 2θ, and θ is half the Bragg angle.

Table 3 demonstrates that the calculated average crystalline sizes were 19.23 nm, 20.20 nm, and 21.82 nm at 550 °C and 27.39 nm, 28.90 nm, and 30.13 nm at 750 °C for SnO_2 samples, when prepared using a solvents medium consisting of methanol, ethylene glycol, and water in the ratios of 50:50:0, 25:25:50, and 0:0:100, respectively. FWHM was measured using Gaussian-Lorentzian fitting in Origin 8.5 software. Fig. 3 and Table 3 show that as the water content of the solvent medium and temperature increased, the diffraction peaks became narrower. This indicates a reduction in FWHM, suggesting that the SnO_2 nanoparticles grew larger crystallite sizes in the nanometer range, accompanied by enhanced crystallization and decreased surface area. The crystalline sizes were increased in the nm range as the water-to-organic ratio of the solvent medium and calcination temperatures increased, as shown in Fig 4. The organic precursor solvent medium samples yielded the smallest crystalline size value of 19.23 nm and 27.39 nm at 550 °C and 750 °C, respectively. In comparison, the samples containing water medium precursor solvents obtained the highest crystalline size value of 20.20 nm, 21.81 nm at 550 °C and 28.90 nm, 30.13 nm at 750 °C, respectively. This phenomenon can be due to these solvents' divergent polar characteristics and dielectric constants. Ethylene glycol and methanol have a lower polarity value than water, which increases the saturation vapour pressure at the same temperature. As a result, greater control will be feasible, and the precipitate rate in methanol and ethylene glycol will be reduced in comparison to water [15]. Based on the preceding discussion, the SnO_2 nanoparticle

sample S1, subjected to calcination at 550 °C, exhibited the smallest average crystallite size of 19.23 nm, with an interplanar d-spacing of 0.3357 nm corresponding to the (110) crystal plane. The pronounced broadening of its diffraction peaks, relative to other samples, indicates significant lattice strain. This strain is attributed to anisotropic crystal growth dynamics and differential nucleation rates across distinct crystallographic planes, as also reported by Preethi et al. [30].

An XRD profile was also employed to ascertain the crystallographic texture coefficient of the synthesized materials. The surface texture ratio offers insights into the material's preferred growth orientation. To calculate the texture coefficient, standard intensities associated with the crystallographic planes were extracted from the standard JCPDS card no. 00-021-1250. The texture coefficient (TC) measures the preferential orientation of crystal planes and was calculated (Table 1) using Eq. 7 [31].

$$T_{(h_i k_i l_i)} = \frac{I_{(h_i k_i l_i)}}{I_{0(h_i k_i l_i)}} \left[\frac{1}{n} \sum_{i=0}^{n} \frac{I_{(h_i k_i l_i)}}{I_{0(h_i k_i l_i)}} \right] \quad (7)$$

Here, $TC_{(hkl)}$ is the texture coefficient for the Miller-indexed plane, $I_{(hkl)}$ imply experimental intensities from the sample, and $I_{o(hkl)}$ corresponds to standard intensities from the JCPDS card. The variable *n* denotes the number of peaks.

Texture coefficients above or below unity suggest a larger (lower) degree of preferred orientation of the growth along a specific plane than bulk SnO_2. Since X-ray intensities depend on atomic structure factors, the texture coefficient's divergence from unity for a particular Miller plane also affects its atomic densities [22]. As seen in Table 2, at 550 ºC calcined temperature, the predominantly oriented growth of SnO_2 samples was observed along high-energy crystal planes (110) and (211). In contrast, minimal growth orientation was observed along low-energy crystal planes (101). In varying proportions, this growth was facilitated by precursor solvents, including methanol, ethylene glycol, and water. Whereas, at 750 ºC, the sample (S1-750) utilised an organic precursor solvent consisting of a methanol: ethylene glycol ratio, which exhibited a preferential direction along the high-energy crystal planes (110) and (211). At the same time, insignificant growth was observed along the low-energy crystal plane (101). On the other hand, samples S2-750 and S3-750, grown in a solvent medium containing water content, preferred the high-energy crystal plane (110) over the lower-energy plane (211). Table 2 summarizes the texture analysis. Consequently, the texture coefficient analysis reveals that the SnO_2 nanoparticles in all samples predominantly grow along the high-energy (110) crystal plane, confirming it as the favoured orientation. The high surface energy of these samples results from crystal growth along high-energy planes, which have more exposed and reactive sites, enhancing their reactivity. The consistent performance was explained by many researchers [22, 23]. Materials with high-energy crystal planes are favoured owing to their enhanced reactivity in the fields of photocatalysis [22].

International Journal of Environmental Sciences
ISSN: 2229-7359
Vol. 11 No. 2, 2025
https://www.theaspd.com/ijes.php

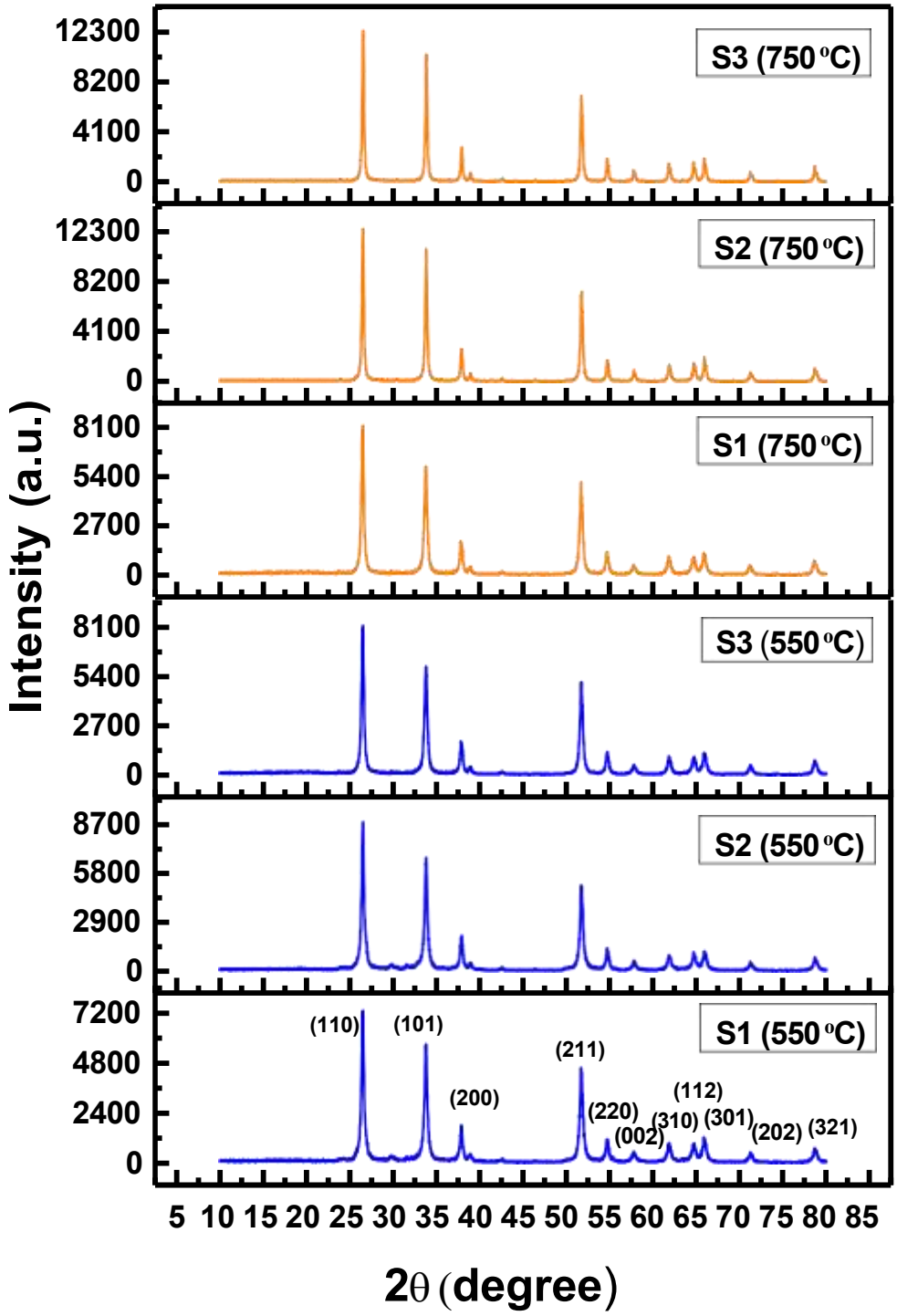

Fig. 3: XRD profiles of S1, S2 and S3 samples of synthesized SnO_2 nanoparticles using different volume ratios of solvents (methanol: ethylene glycol: water) at 550 °C and 750 °C, respectively.

Table 2: Texture coefficient (P_{hkl}) values for SnO_2 nanoparticles, synthesized with different solvent ratios (methanol: ethylene glycol: water) and calcined at 550 °C and 750 °C, respectively, were calculated to assess the preferred crystallographic growth direction and structural alignment.

Plane (hkl)	**Texture Coefficient (P_{hkl})**					
	Calcination temperature at 550 ºC			**Calcination temperature at 750 ºC**		
	S1-550 (50:50:0)	**S2-550 (25:25:0)**	**S3-550 (0:0:100)**	**S1-750 (50:50:0)**	**S2-750 (25:25:0)**	**S3-750 (0:0:100)**
110	1.03336	1.05064	1.04685	1.00205	1.00044	1.02375
101	0.96503	0.96633	0.92799	0.98891	1.05293	1.05521
211	1.0016	0.98301	1.02515	1.00902	0.94662	0.92102

Table 3: Calculated crystallographic parameters derived from XRD pattern and particle size derived from FESEM of synthesized SnO_2 nanoparticles by using distinct solvent mixture ratios (methanol: ethylene-glycol: water) and calcined at temperatures of 550°C and 750°C, respectively.

Calcination Temperatures (ºC)		**550 ºC**			**750 ºC**		
Experiment code with different solvent ratios		**S1-550 (50:50:0)**	**S2-550 (25:25:0)**	**S3-550 (0:0:100)**	**S1-750 (50:50:0)**	**S2-750 (25:25:0)**	**S3-750 (0:0:100)**
2θ (degree)		26.51	26.53	26.51	26.49	26.53	26.58
FWHM (radian)		0.0074	0.0070	0.0065	0.0051	0.0049	0.0047
d-spacing (nm)		0.3357	0.3356	0.3357	0.3361	0.3355	0.3349
Lattice parameters	**a (nm)**	0.4748	0.4746	0.4748	0.4753	0.4745	0.4737
	c (nm)	0.3192	0.3185	0.3192	0.3194	0.3186	0.3183
c/a ratio		0.6722	0.6710	0.6719	0.6721	0.6714	0.6718
Unit volume ($Å^3$)		71.97	71.75	72.16	71.98	71.73	71.44
No. of unit cell (x 10^3)		51.70	60.14	148.97	75.49	176.08	200.39
Dislocation density (lines/m^2) (x 10^{15})		2.70	2.44	1.33	2.10	1.19	1.10
Average crystalline size (D) (nm)		19.23	20.20	21.82	27.39	28.90	30.13
Average particle size by FESEM (nm)		29.21	30.23	32.52	31.95	33.69	40.13

International Journal of Environmental Sciences
ISSN: 2229-7359
Vol. 11 No. 2, 2025
https://www.theaspd.com/ijes.php

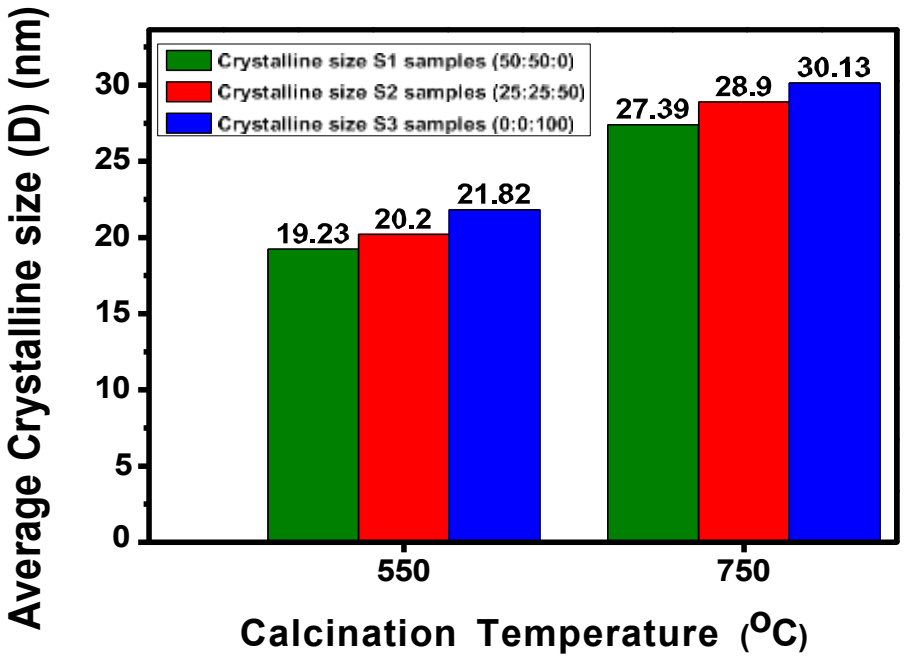

Fig. 4: Variation of the crystalline size of all SnO_2 nanoparticle samples with different volume ratios of solvents (Methanol: Ethylene glycol: DDW) at 550 ºC and 750 ºC calcination temperatures, respectively.

3.2 Morphological studies

Surface morphology investigations of synthesised SnO_2 nanoparticles were analysed using FESEM images at 1µm magnification to determine particle size and texture. FESEM micrographs demonstrating the powder synthesized samples of SnO_2 nanoparticles in different solvents (Methanol: Ethylene glycol: DDW) containing volume ratios of 50:50:0, 25:25:50, and 0:0:100 under calcination conditions of 550 °C and 750 °C, respectively as shown in Fig 5. As can be seen from the FESEM graphs (Fig. 5a-f), all images showed the changes in morphology from an irregular spherical shape with less agglomerated to highly agglomerated when calcined at 550 °C and 750 °C, when the volume ratio of water solvent increased. As a result, the particle size increased from 29.21 nm to 32.52 nm at 550 ºC and from 31.95 nm to 40.13 nm at 750 ºC of SnO_2 nanostructure as water-mediated content increased (Table 3). Data presented in Table 3 and Fig.5 showed that all samples had non-uniform particle sizes and varying degrees of agglomeration. This may indicate primary particle clustering to generate bigger particles. The grain size distribution and agglomeration depend on nucleation and growth rates [32]. Furthermore, water-mediated solvent samples produce larger particles with greater agglomeration than organic-mediated solvent samples, which tend to produce less agglomeration and smaller particles at 550 ºC and 750 ºC. This is because the dispersal capability of organic solvents is superior to that of aqueous media, which significantly amplifies the aggregation effect in aqueous media [33]. Table 2 illustrates that the FESEM images match well with the XRD data, which are influenced by the nucleation and growth rate mechanism that contribute to aggregation and lead to changes in the granular dimensions and the surface morphology of all nanostructured SnO_2. From the above results, the organic-mediated solvent sample (S1-550) of SnO_2 nanoparticles was found to be irregularly spherical among some tiny rods with less agglomerated morphology of small average particle size about~29.21 nm range at 550 ºC than other samples. Smaller particle size and morphology suggest organic solvents regulate nucleation and crystal orientation.

International Journal of Environmental Sciences
ISSN: 2229-7359
Vol. 11 No. 2, 2025
https://www.theaspd.com/ijes.php

Possible growth mechanism of SnO_2 nanoparticles:

SnO_2 morphological alterations and particle size during chemical reactions were primarily affected by volume ratios of solvents (methanol: ethylene glycol: water) and calcination temperature. The possible reaction mechanism can be depicted as:

$$SnCl_2 + 2\ CH_3OH \rightarrow Sn(OH)_2 \downarrow + 2CH_3Cl \quad (8)$$

$$Sn(OH)_2 = SnO + 2H_2O \quad (9)$$

$$SnO + O_2 \leftrightarrow 2SnO_2 \quad (10)$$

Solvents are instrumental in controlling the reaction mechanism, thereby impacting the efficiency and outcome of product synthesis. The morphology of a crystal is dictated by the differential growth rates of its crystallographic planes, which are strongly influenced by variations in surface free energy. SnO_2 crystals are generated through a nucleation and growth process, with the formation of SnO_2 being a by-product of the reaction of $Sn(OH)_2$ (Eq. 8-10). When the solvent has low polarity, the process of hydrolysis slows down, resulting in the production of fewer $Sn(OH)_2$ growth units and the formation of nanoparticles with smaller dimensions. Consequently, bigger particles with faster growth rates are generated in aqueous media due to increased hydrolysis as compared to organic media (methanol, ethylene glycol). In simple terms, the organic medium yields smaller SnO_2 particles [15].

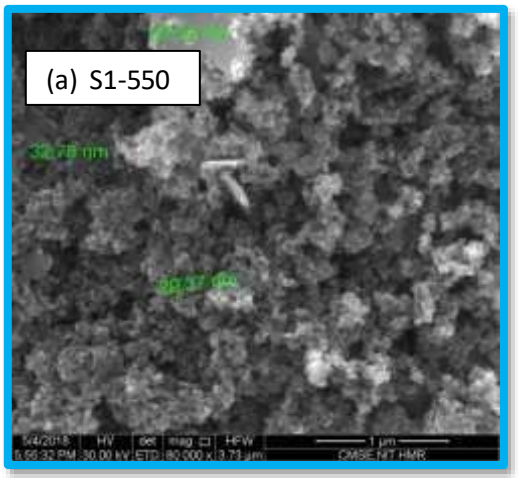

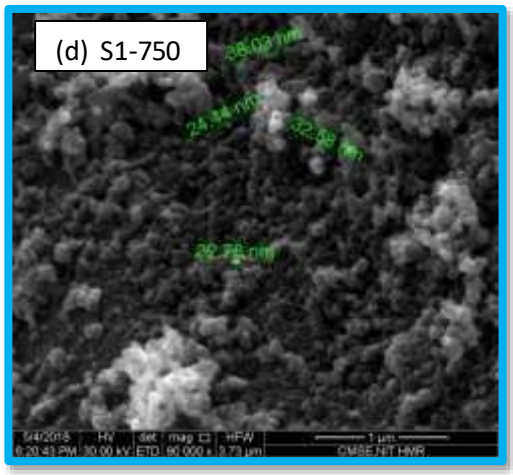

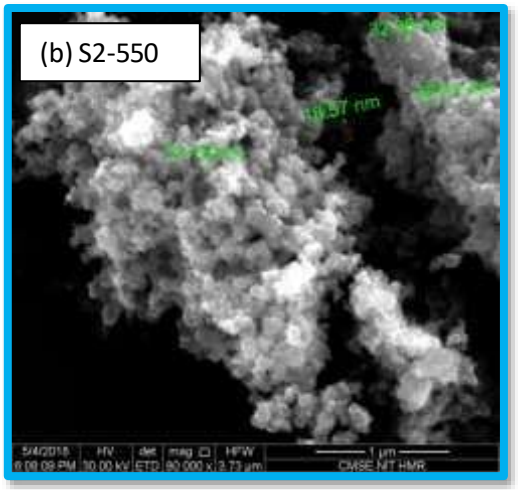

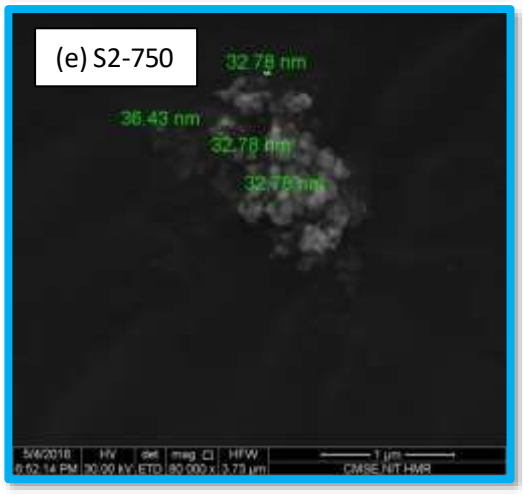

International Journal of Environmental Sciences
ISSN: 2229-7359
Vol. 11 No. 2, 2025
https://www.theaspd.com/ijes.php

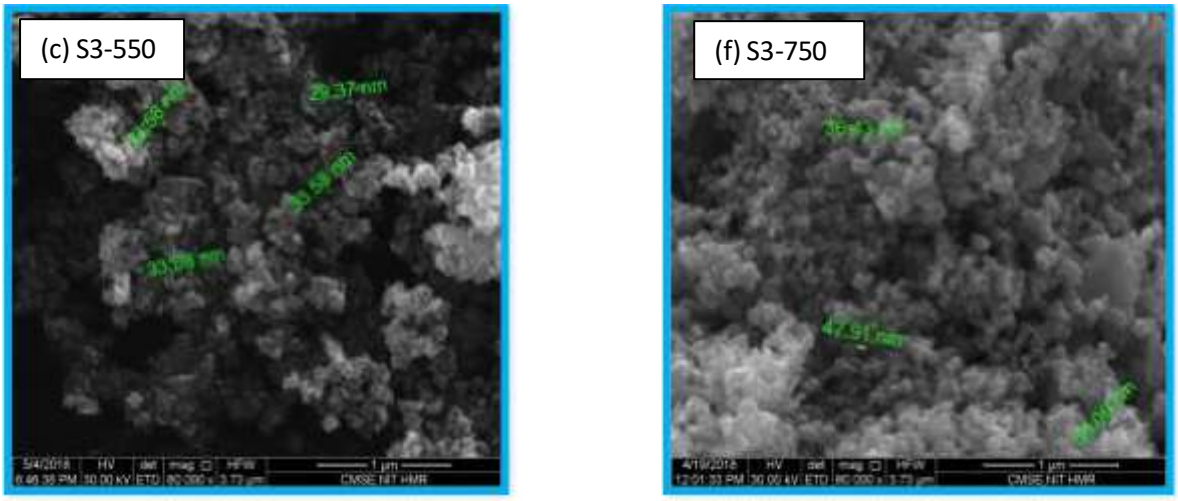

Fig. 5: FESEM images of all SnO_2 nanoparticles with different solvents (Methanol: Ethylene glycol: DDW) containing volume ratios of 50:50:0 (a-d), 25:25:50 (b-e), and 0:0:100 (c-f) at 550 ºC and 750 ºC, respectively.

3.3 Dispersion studies (EDX)

Material elemental composition and purity were analysed using EDX to detect element presence. Fig. 6 illustrates that the Energy-Dispersive X-ray (EDX) analysis provided quantitative compositional data, revealing a weight percentage of 79.88% for tin (Sn) and 20.12% for oxygen (O). This suggests a high proportion of tin in the material. Furthermore, the atomic percentage composition of the nanoparticles was found to be 49.28% for Sn and 50.72% for O, as depicted in Fig. 6, confirming the near-stoichiometric ratio of tin and oxygen in the sample. The EDX spectrum data clearly show distinct peaks corresponding to the tin (Sn) and oxygen (O) elements, confirming their high abundance in the synthesized SnO_2 samples. The absence of any additional peaks in the spectra further supports the purity of the material, indicating no significant contamination or the presence of unwanted phases.

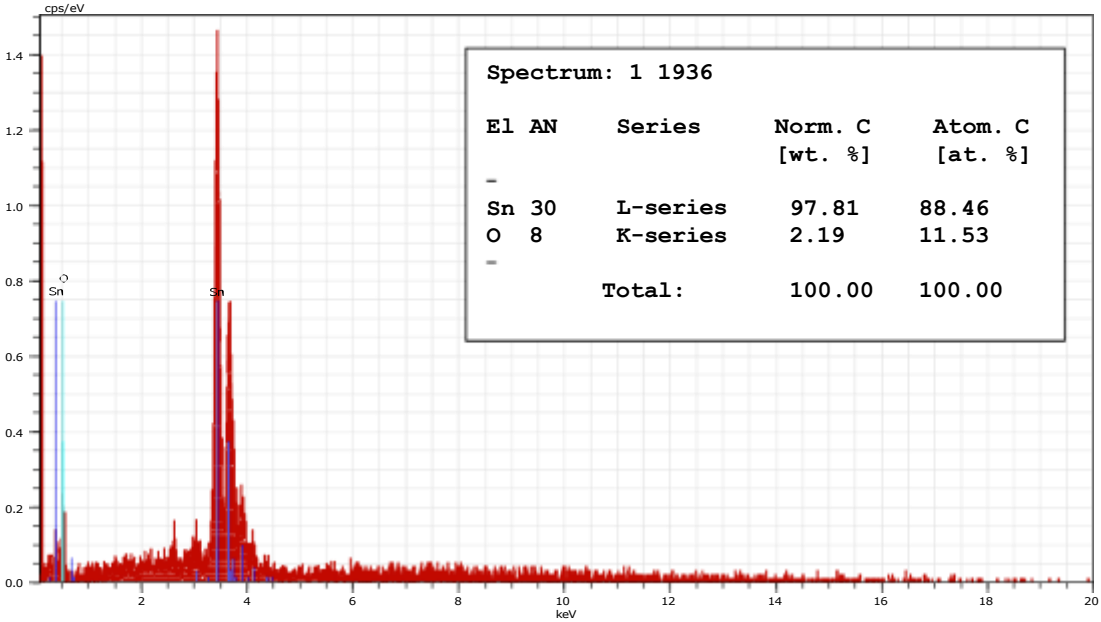

Fig. 6: EDX analysis of SnO_2 (S1-550), prepared at 550 °C with a 50:50:0 solvent mix (Methanol: Ethylene glycol: DDW)

International Journal of Environmental Sciences
ISSN: 2229-7359
Vol. 11 No. 2, 2025
https://www.theaspd.com/ijes.php

3. 4. IR spectroscopy studies

FTIR analysis was used to monitor functional groups, identify unknown substances, and analyse chemical bonding. Synthesised tin oxide (SnO_2) nanoparticles samples were categorised by functional group and formation using IR spectra wave-numbers range from 400 cm^{-1} to 4000 cm^{-1} nanoparticles with different solvents (Methanol: ethylene glycol: DDW) containing volume ratios of 50:50:0, 25:25:50, and 0:0:100 corresponding to calcination at 550 °C and 750 °C, respectively, as shown in Fig 7. The broad absorption bands for all SnO2 samples emerged from this spectrum in the 3422 to 3444 cm^{-1} range, attributed to the O–H stretching vibration of surface-adsorbed water molecules on SnO_2 [34]. In addition, the minor peaks within the 2800-2925 cm^{-1} range indicated the presence of the C-H functional group [35]. Absorption bands near 1630-1640 cm^{-1} are ascribed to the bending vibration of O–H groups from water molecules entrapped within the nanostructure SnO_2 samples [36]. The absorption peaks in the vicinity of 1051-1057 cm^{-1} were attributed to the C-N stretching mode, demonstrating surface adsorption behaviour consistent across all SnO_2 samples [35]. The FTIR spectra display a strong and sharp absorption peak for all SnO_2 samples within a range of 622 to 668 cm^{-1}. The observed peak can be assigned to the Sn-O-Sn stretching vibration mode in the surface bridging oxide of $Sn(OH)_4$. This oxide is generated through the condensation of hydroxyl group vibrations on adjacent surfaces [36, 37]. Such a mode in the synthesized samples confirms that SnO_2 is formed as crystalline phase. However, the observed shift in wavenumber may result from changes in band intensity caused by increased water-based solvent content and elevated calcination temperatures, leading to the removal of residual OH groups, unreacted organics, and adsorbed species from the SnO_2 surface.

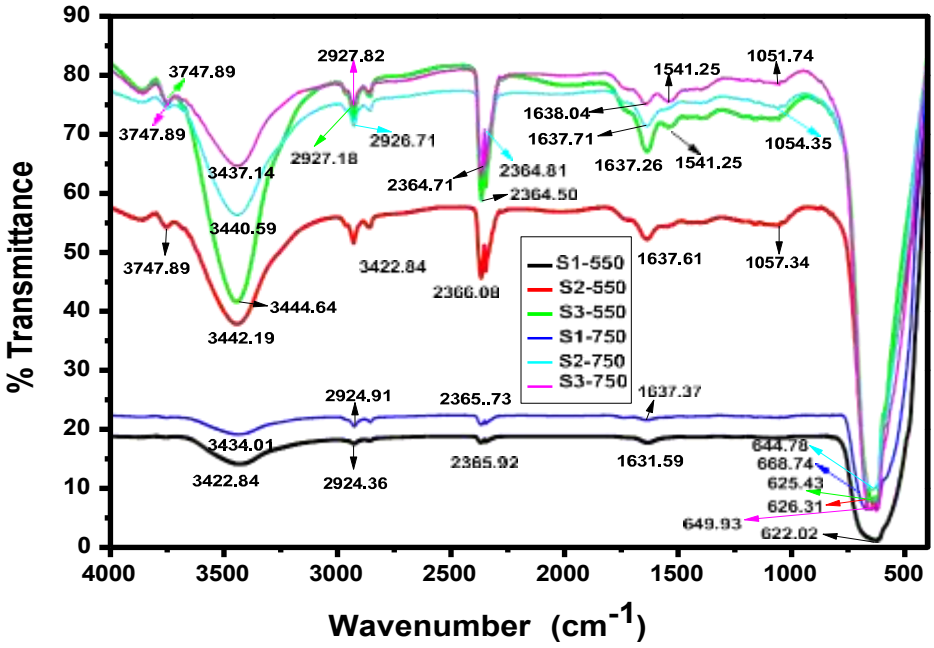

Fig. 7: Comparison of FTIR spectra of SnO_2 nanoparticles (S1, S2, S3) prepared with distinct solvent mixtures (methanol: ethylene glycol: water) at 550 ºC and 750 ºC, respectively.

3. 5. Optical analysis

DRS-UV-Vis spectroscopy was used to measure the optical bandgap of SnO_2 nanoparticles samples at 550 ºC and 750 ºC with different solvents (methanol: ethylene glycol: water) containing volume ratios of 50:50:0, 25:25:50, and 0:0:100, respectively. Two different approaches are available for calculating

The optical bandgap of SnO_2 samples.
(a) The equation for energy wavelength is as follows (eq.11) [38]:

$$Eg = \frac{1240}{\lambda} \text{ (eV)} \quad (11)$$

b) Apply Tauc's Plot absorption spectra fitting technique by extrapolating the linear section of $(\alpha h\nu)^2$ vs $h\nu$ plot (Fig.8 (a-b)). Tauc's formula (Eq.12) was utilised for direct transition [39].

$$(\alpha h\nu) = B(h\nu - E_g)^n \quad (12)$$

Where, λ = wavelength in nm, the symbol α represents the absorption coefficient, B denotes a constant associated with the effective masses of the bonds, Eg signifies the real optical energy bandgap (eV), and $h\nu$ implies the energy of incident photons. The nature of the transitions determines the value of n: 2 indicate allowed indirect transitions, 1/2 indicates direct transitions, and 3 and 3/2 signify forbidden indirect transitions and direct transitions, respectively.

As illustrated in Fig. 8 (a-b), a graph representing the relationship between incident wavelength (λ) (nm) and absorbance (A) (a.u.) for all synthesised SnO_2 nanoparticles samples reveals a shift in the cut-off wavelength were increased 377 nm, 472 nm, and 477 nm at 550 ºC and 394 nm, 401 nm and 404 nm at 750 ºC when the volume ratio of water solvent increased, respectively. These values are larger than the reported value of 344 nm for bulk SnO_2. The DRS spectra demonstrate a shift in the maximum absorption towards longer wavelengths, signifying a red shift of the absorption edge into the near-infrared region, which suggests alterations in the electronic structure and band gap of the material. This shift has influenced the optical bandgap transition and particle diameters. The optical band gap values derived from both equations have been summarized and are presented in Table 4 for comparison. The measured Tauc's plot band gap energies were found to be 3.73 eV, 3.03 eV, and 2.94 eV at 550ºC and 3.72 eV, 3.68 eV, and 3.59 eV at 750ºC for SnO_2 samples (S1, S2, S3 respectively) prepared using a solvent medium consisting of methanol, ethylene glycol, and water in the ratios of 50:50:0, 25:25:50, and 0:0:100 respectively. As the water content in the solvent medium increased, the optical bandgap decreased from 3.73 eV to 2.90 eV at 550 °C and from 3.72 eV to 3.59 eV at 750 °C, subsequently rising at elevated calcination temperatures. The observed variation in bandgap energies may be attributed to the distortions induced in the crystalline lattice of SnO_2 [6]. In other words, the bandgap energy tended to increase as the amount of organic content (methanol and ethylene glycol) in the solvent medium increased. This is because the particle size is decreased at shorter wavelengths [40], supporting the findings from XRD, FESEM and FTIR. The findings of other researchers have reached the same conclusions [15, 23].

Fig. 8 (a-b) illustrates that the UV–visible spectrum of the as-prepared organic-mediated (methanol: ethylene glycol) SnO_2 nanoparticles samples exhibits band gap energies of 3.73 eV at 550 °C and 3.72 eV at 750 °C, both exceeding the bulk SnO_2 value of 3.6 eV. In contrast, the band gap observed for the water-mediated solvent samples is 2.94 eV at 550 °C and 3.59 eV at 750 °C, which is lower than that of bulk SnO_2. The potential factors contributing to variances in the optical bandgap of rutile oxide are delineated as follows: many causes account for the bandgap differences. One probable explanation is the less significant prevalence of quantum confinement in nanoparticles, a result of their crystalline size, because the band gap energy of all SnO_2 samples shows a 0.1 eV red shift compared to bulk SnO_2. When the particle size is on the order of Bohr's radius, quantum confinement and coulomb correlation significantly modify the excitation energy, affecting the electronic transitions across the entire band [35]. It is evident that the optical bandgap energy (Eg) of all SnO_2 nanoparticles is minimally influenced by the organic-water-mediated solvents at calcination temperatures; the outcomes of quantum confinement have a negligible impact on altering the bandgap level.

International Journal of Environmental Sciences
ISSN: 2229-7359
Vol. 11 No. 2, 2025
https://www.theaspd.com/ijes.php

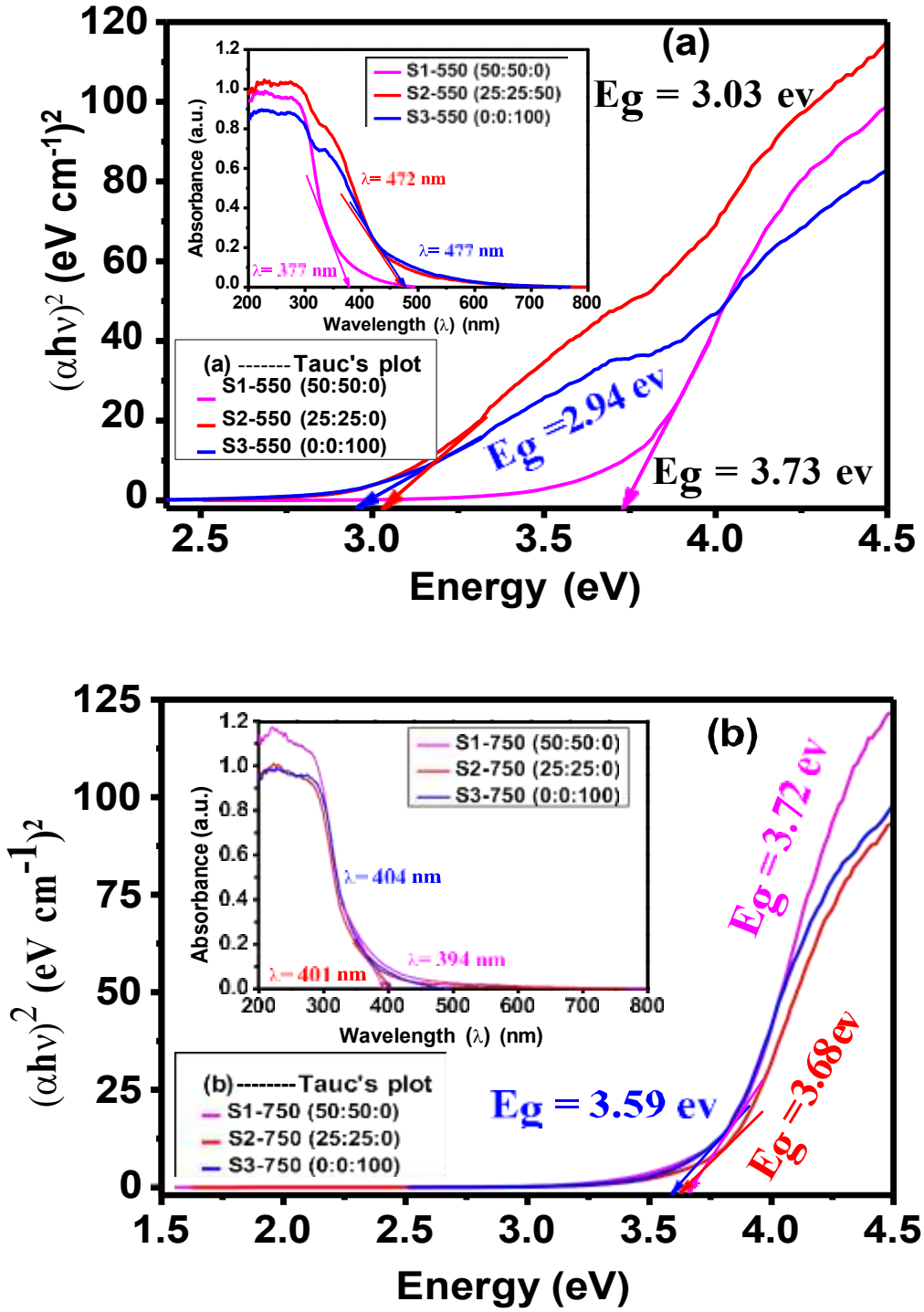

Fig. 8: Reflectance spectra analysis shows cut-off absorption and optical energy gap by Tauc's graphical method for Tin oxide (SnO_2) nanoparticles samples (S1, S2, S3) with different volume ratio of solvents (methanol: ethylene glycol: water) at (a) 550 ºC and (b) 750 ºC.

Table 4: The energy band gap of SnO_2 nanoparticles samples was evaluated by analysing their spectral absorption curve.

Test code	**Calcination temperatures**	**Cut-off wavelength (λ) (nm)**	**Optical energy gap (E_g) (by Equation) (eV)**	**Tauc's band gap plot (eV)**
S1-550	550 ° C	377	3.28	3.73
S2-550		472	2.62	3.03
S3-550		477	2.59	2.94
S1-750	750 ° C	394	3.14	3.72
S2-750		401	3.09	3.68
S3-750		404	3.06	3.59

Table 5: An assessment of different techniques for synthesizing SnO_2 nanoparticles.

Sr. No.	**Processing technique**	**Given conditions**	**Nanostructures**	**Appearance**	**Mean crystalline size(nm)**	**Literature**
1.	Chemical Co-Precipitation	Precursor Solvents: pentanol, formamide, butanol, ethanol, propanol, acetonitrile, and water	SnO_2	Irregular shape and highly agglomerated	15-20	[11]
2.	Microwave irradiation	Precursor Solvents: acetone, ethanol, and water	HDA-Capped ZnO	Spheres, rods and stars shape	45-100	[14]
3.	Hydrothermal	Precursor Solvents: water and methanol; Mineralisers: NaOH and KOH	ZnO	Nanorods shape	40.4	[15]
4.	Sol-gel	Ethanol to water solvent medium	ZnO	Spherical to tiny rods shape	10.80-28.10	[16]
5.	Solvothermal	Mixed Solvents: Ethylenediamine and distilled water	ZnS	Nanorod shape	Band-gap 3.49 -3.74 (eV)	[21]
6.	Spray pyrolysis	Precursor Solvents: H_2O_2, water, Isopropanol, 1-propanol, methanol, and	SnO_2	Mat-like to thin film nanostructures	5.9-20.5	[22]

		Ethanol				
7.	Co-Precipitation	Methanol to Water solvent medium	SnO_2	Spherical shape	10-17	[23]
8.	Chemical	polar-protic and polar-aprotic solvents	CTAB-Ag	Irregular and agglomerated grains shape	Absorbance (1.06-014 a.u.)	[24]
9.	Precipitation	Precursor Solvents: De-ionized, Isopropyl ethanol, and water	SnO_2	Agglomeration nanostructures	6-23	[27]
10.	Sol-gel	Precursor Solvents: methanol, ethanol, and water	SnO_2	Spherical shape	3.9 to 5.0	[41]
11.	**Sol-gel Calcination**	**Organic to water medium ratio at 550 ºC and 750 ºC calcination temperatures**	**SnO_2**	**Spherical shapewith tiny rods**	**19.23-21.82 at 550 ºC and 27.39-30.13 at 750 ºC**	**Present study**

CONCLUSIONS

The study demonstrates that solvent polarity and calcination temperature play crucial roles in tailoring the structural, morphological, and optical properties of SnO_2 nanoparticles synthesized via sol-gel calcination. All samples exhibited a well-defined tetragonal rutile structure with a dominant (110) orientation. Smaller, less agglomerated particles formed in organic-rich solvents, while water-rich systems led to larger, clustered morphologies. Notably, the S1-550 sample derived from a methanol + ethylene glycol solvent system, produced the most desirable morphology—fine, uniform, and minimally agglomerated particles, making it highly promising for enhanced photocatalytic activity. This study highlights the crucial role of solvent polarity in tuning nanoparticle growth, structure, and function.

Acknowledgements
This study was performed with UGC's aid in New Delhi. NIT Hamirpur provided FESEM and EDX characterisation help; the authors would be pleased. DRS Spectra laboratory analysis is grateful to the Department of Environment Science, Thapar University, Patiala, for its scientific help. The authors further appreciate the Department of Physics, GJUS&T, Hisar, for the XRD study facility and the Central Lab for the FTIR equipment.

REFERENCES

[1] Zebbar, N., Aida, M. S., Hafdallah, A. E. K., Daranfad, O., Lekiket, H., and Kechouane, M. (2009). Properties of ZnO thin films grown on Si substrates by ultrasonic spray and ZnO/Si heterojunctions. In *Materials Science Forum, 609*, 133-137 Trans Tech Publications Ltd.

[2] Bilgin, V. İ. L. D. A. N., Akyuz, I., Ketenci, E., Kose, S., and Atay, F. E. R. H. U. N. D. E. (2010). Electrical, structural and surface properties of fluorine doped tin oxide films. *Applied Surface Science*, *256(22),* 6586-6591.

[3] Roguai, S., and Djelloul, A. (2022). Structural and optical analysis of SnO_2 thin films by spray pyrolysis. *Algerian Journal of Environmental Science and Technology*, *8*(1), 2285-2290.

[4] Mondal, I., Kiruthika, S., Ganesha, M. K., Baral, M., Kumar, A., Vimala, S., and Kulkarni, G. U. (2021). ITO-free large area PDLC smart windows: a cost-effective fabrication using spray coated SnO_2 on an invisible Al mesh. *Journal of Materials Chemistry A*, *9*(40), 23157-23168.

[5] Das, S., and Jayaraman, V. (2014). SnO_2: A comprehensive review on structures and gas sensors. *Progress in Materials Science*, *66*, 112-255.

[6] Roguai, S., and Djelloul, A. (2022). Structural, morphological, optical and electrical properties of Ni-doped SnO_2 thin films by pneumatic spray pyrolysis method. *Bulletin of Materials Science*, *45*(4), 227.

[7] Nejati-Moghadam, L., Ghanbari, D., Salavati-Niasari, M., Esmaeili-Bafghi-Karimabad, A., and Gholamrezaei, S. (2015). Photo-degradation of organic dyes: simple chemical synthesis of various morphologies of tin dioxide semiconductor and its nanocomposite. *Journal of Materials Science: Materials in Electronics*, *26*, 6075-6085.

[8] Shen, Y., Cao, X., Zhang, B., Wei, D., Ma, J., Liu, W., and Shen, Y. (2014). Synthesis of SnO_2 nanorods and application to H2 sensor. *Journal of alloys and compounds*, *593*, 271-274.

[9] Yong, S. M., Tsvetkov, N., Larina, L., Ahn, B. T., and Kim, D. K. (2014). Ultrathin SnO_2 layer for efficient carrier collection in dye-sensitized solar cells. *Thin Solid Films*, *556*, 503-508.

[10] Park, H., Lee, J., Kim, H., Kim, D., Raja, J., and Yi, J. (2013). Influence of SnO_2: F/ZnO: Al bi-layer as a front electrode on the properties of pin amorphous silicon based thin film solar cells. *Applied Physics Letters*, *102*(19).

[11] Horti, N. C., Kamatagi, M. D., Patil, N. R., Wari, M. N., and Inamdar, S. R. (2018). Photoluminescence properties of SnO_2 nanoparticles: effect of solvents. *Optik*, *169*, 314-320.

[12] Khaenamkaew, P., Manop, D., Tanghengjaroen, C., and Palakawong Na Ayuthaya, W. (2020). Crystal structure, lattice strain, morphology, and electrical properties of SnO_2 nanoparticles induced by low calcination temperature. *Advances in Materials Science and Engineering*, *2020*, 1-10.

[13]. Guo, Q., Chen, S., and Qin, X. (2014). Preparation of graphene/SnO_2 composite as high capacity anode material for lithium ion batteries. *Materials Letters*, *119*, 4-7.

[14] Khoza, P. B., Moloto, M. J., and Sikhwivhilu, L. M. (2012). The effect of solvents, acetone, water, and ethanol, on the morphological and optical properties of ZnO nanoparticles prepared by microwave. *Journal of Nanotechnology*, *2012*, 1-6.

[15] Edalati, K., Shakiba, A., Vahdati-Khaki, J., and Zebarjad, S. M. (2016). Low-temperature hydrothermal synthesis of ZnO nanorods: Effects of zinc salt concentration, various solvents and alkaline mineralizers. *Materials Research Bulletin*, *74*, 374-379.

[16] Ungula, J., and Dejene, B. F. (2016). Effect of solvent medium on the structural, morphological and optical properties of ZnO nanoparticles synthesized by the sol–gel method. *Physica B: Condensed Matter*, *480*, 26-30.

[17] Shaaban, E. R., Mostafa, A. M. A., Hassan, H. S., Abd El-Sadek, M. S., and Mohamed, G. Y. (2014). Effect of γ-irradiation on Structural and Optical Ellipsometry Parameters of ZnO

Nanocrystalline Thin Films. *International Journal of Thin Film Science and Technology*, *3(3),* 129-141.

[18] Akhir, M. A., Mohamed, K., Lee, H. L., and Rezan, S. A. (2016). Synthesis of tin oxide nanostructures using hydrothermal method and optimization of its crystal size by using statistical design of experiment. *Procedia Chemistry*, *19*, 993-998.

[19] Imran, M., Riaz, S., and Naseem, S. (2015). Synthesis and characterization of titania nanoparticles by sol-gel technique. *Materials Today: Proceedings*, *2(10),* 5455-5461.

[20] Sood, S., Umar, A., Mehta, S. K., and Kansal, S. K. (2015). Highly effective Fe-doped TiO_2 nanoparticles photocatalysts for visible-light driven photocatalytic degradation of toxic organic compounds. *Journal of colloid and interface science*, *450*, 213-223.

[21] Mendil, R., Ayadi, Z. B., and Djessas, K. (2016). Effect of solvent medium on the structural, morphological and optical properties of ZnS nanoparticles synthesized by solvothermal route. *Journal of Alloys and Compounds*, *678*, 87-92.

[22] Paloly, A. R., and Bushiri, M. J. (2021). The effect of solvents on the growth and key properties of tin oxide thin films deposited via chemical spray pyrolysis. *Materials Chemistry and Physics*, *261*, 124209.

[23] Kumar, V., Singh, K., Kumar, A., Kumar, M., Singh, K., Vij, A., and Thakur, A. (2017). Effect of solvent on crystallographic, morphological and optical properties of SnO_2 nanoparticles. *Materials Research Bulletin*, *85*, 202-208.

[24] Khan, Z., Al-Thabaiti, S. A., Obaid, A. Y., Khan, Z. A., and Al-Youbi, A. O. (2011). Effects of solvents on the stability and morphology of CTAB-stabilized silver nanoparticles. *Colloids and Surfaces A: Physicochemical and Engineering Aspects*, *390*(1-3), 120-125.

[25] Saravanan N., Ponnusamy S., Shri Prasad S. and Joseph V. (2014): Synthesis and characterization of SnO_2 quantum dots. *International Journal of Chemtech Research*. *6(1):* 600-603.

[26] Reddy, A. R., Mallika, A. N., Babu, K. S., and Reddy, K. V. (2015). Hydrothermal synthesis and characterization of ZnO nanocrystals. *International Journal of Mining, Metallurgy & Mechanical Engineering*, *3(2),* 2320-4060.

[27] Chand, P. (2020). Optical and photocatalytic response to solvent-based synthesis of SnO_2 nanostructures. *Materials Today: Proceedings*, *28*, 188-192.

[28] Gaber, A., Abdel-Rahim, M. A., Abdel-Latief, A. Y., and Abdel-Salam, M. N. (2014). Influence of calcination temperature on the structure and porosity of nanocrystalline SnO_2 synthesized by a conventional precipitation method. *International Journal of Electrochemical Science*, *9*(1), 81-95.

[29] Rangari, N. G. (2018). Investigation of Structural and Optical Properties of SnO_2 Nano-rod by Sol-gel technique. *IJSRST (4) 5* : 1618-1622.

[30] Preethi, S., Anitha, A., and Arulmozhi, M. (2016). A comparative analysis of the properties of zinc oxide (ZnO) nanoparticles synthesized by hydrothermal and sol–gel methods. *Indian Journal of Science and Technology*, *9(40),* 1-6.

[31] Singh, P., Kaur, G., Singh, K., Singh, B., Kaur, M., Kaur, M., and Kumar, A. (2018). Specially designed B_4C/SnO_2 nanocomposite for photocatalysis: traditional ceramic with unique properties. *Applied Nanoscience*, *8*, 1-9.

[32] Habte, A. G., Hone, F. G., and Dejene, F. B. (2022). Influence of Cu-Doping Concentration on the Structural and Optical Properties of SnO_2 Nanoparticles by Coprecipitation Route. *Journal of Nanomaterials*, *2022*. 1-10.

[33] Anandan, K., and Rajendran, V. (2010). Solvents effect of quantum sized SnO_2 nanoparticles via solvothermal process and optical properties. *Material. Science. Resource. India*, *7*(2), 389-397.

[34] Chand, P. (2019). Effect of pH values on the structural, optical and electrical properties of SnO_2 nanostructures. *Optik*, *181*, 768-778.

[35] Arif, H. S., Murtaza, G., Hanif, H., Ali, H. S., Yaseen, M., and Khalid, N. R. (2017). Effect of La on structural and photocatalytic activity of SnO_2 nanoparticles under UV irradiation. *Journal of Environmental Chemical Engineering*, *5(4),* 3844-3851.

[36] Drzymała, E., Gruzeł, G., Depciuch, J., Budziak, A., Kowal, A., and Parlinska-Wojtan, M. (2017). Structural, chemical and optical properties of SnO_2 NPs obtained by three different synthesis routes. *Journal of Physics and Chemistry of Solids*, *107*, 100-107.

[37] Aziz, M., Abbas, S. S., Baharom, W. R. W., and Mahmud, W. Z. W. (2012). Structure of SnO_2 nanoparticles by sol–gel method. *Materials Letters*, *74*, 62-64.

[38] Josun, J., Sharma, P., and Garg, V. K. (2024). Optical and structural behavior of hydrothermally synthesized ZnO nanoparticles at various temperatures with NaOH molar ratios. *Results in Optics*, *14*, 100601.

[39] Larbah, Y., Rahal, B. A. D. I. S., and Adnane, M. (2020). The effect of fluorine doping on the properties of SnO_2 thin films deposited using spray pyrolysis method. *Journal of Optoelectronics and Advanced Materials*, *22*(9-10), 518-522.

[40] Bhagwat, A. D., Sawant, S. S., Ankamwar, B. G., and Mahajan, C. M. (2015). Synthesis of nanostructured tin oxide (SnO_2) powders and thin films by sol-gel method. *J. Nano-Electron. Phys*, *7*(4), 04037.

[41] Gnanam, S., and Rajendran, V. (2010). Synthesis of tin oxide nanoparticles by sol–gel process: effect of solvents on the optical properties. *Journal of sol-gel science and technology*, *53*, 555-559.